Iraqi Journal of Scientific and Industrial Research
Volume 2, Issue (3), July-September 2023, pp. 48-55

Spatial Distribution of Magnetic Field in Dual Magnetrons Assembly for Plasma Confinement Applications

Oday A. HAMMADI

Department of Physics, College of Education, Al-Iraqia University, Baghdad, IRAQ

Abstract

In this work, the spatial distribution of the magnetic field between two magnetrons in a closed-field unbalanced dual magnetron system was studied. The magnetic field was measured as a function of the position along the circumference of the circular surface of one magnetron. As well, the variation of magnetic field intensity along the vertical distance separating the two magnetrons was determined. A strategy was proposed for the measurement of the variation of magnetic field intensity at 4 cm away from the electrode surface along four axes. The spatial distribution of the magnetic field intensity over the magnetron surface at 4cm was determined and analyzed.

***Keywords*:** Magnetic field; Discharge plasma; Magnetized plasma; Magnetron

Received: 12 January 2023; **Revised:** 23 April 2023; **Accepted:** 30 April 2023; **Published:** 1 July 2023

1. Introduction

It still difficult to uniformly coat complex components at acceptable rates from a single source despite the advantages of unbalanced magnetrons [1]. Therefore, multiple magnetron systems were supposed to solve such difficulty in order to exploit this technique at commercial levels [2]. In a multiple magnetron system, the magnetic arrays in adjacent magnetrons can be configured with either identical or opposite magnetic polarities [3]. In the first case (identical polarities), the configuration is described as "mirrored" while in the second case (opposite polarities), the configuration is described as "closed-field" [4]. Both configurations are shown in the figure (1).

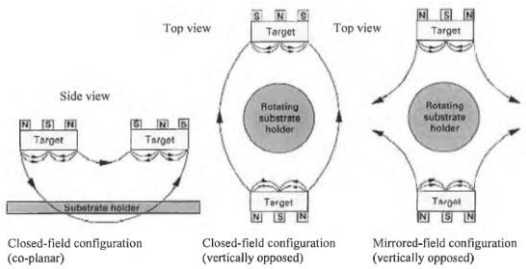

Fig. (1) Different closed-field unbalanced magnetron configurations [5]

In the mirrored configuration, the lines of magnetic field are directed to the walls of the vacuum or deposition chamber and the secondary electrons following these lines are lost, which causes to reduce the plasma density in the substrate region [6-9]. In the closed-field configuration, the lines of magnetic field are linked between the magnetrons, therefore, losses of secondary electrons towards the walls of chamber are low and the substrate is immersed in the high-density plasma region [10]. The advantage of this configuration compared to the mirrored one is realized by the ion-to-atom ratio incident at the substrate (2-3 times greater) at the same conditions [11]. This advantage is observed when comparing to single unbalanced magnetron configuration as well as when the distance from the target is increased [12-15].

Accordingly, the major advantages of closed-field unbalanced magnetrons are high uniformity of the deposited film thickness, high stability of deposition rate for >100 hours uninterrupted production, good reproducibility of layer properties for long periods of time, good adhesion and high density of deposited coatings, the ability to deposit all kinds of metals including high melting-point metals, metal alloys and compounds with precise control of coating composition, the ability to deposit metal oxides, nitrides, carbides, etc. with precise

control of layer stoichiometry, and the ability to deposit tailored design coatings like multicomponent, multilayer, gradient, composite coating, etc. [16-30].

For mode comparison of conventional magnetron, unbalanced magnetron, traditional electromagnetic coil and also with results obtained for other magnetron designs, some additional parameters characterizing the degree of magnetic field unbalance are necessary [31]. For a quantitative estimation of the degree of magnetic field unbalance we have introduced a coefficient of unbalance and a coefficient of geometrical unbalance, characterizing the configuration of the magnetic field above the target surface and, hence, the value of ion current drawn at the substrate [32-35].

For a UBM with a single magnetic system, the coefficient of unbalance K is the ratio of magnetic fluxes from the central and peripheral magnets on the target surface [36]:

$$K = \frac{\Phi_1}{\Phi_2} = \frac{\int_{S_1} B_{\perp 1} dS}{\int_{S_2} B_{\perp 2} dS} \quad (1)$$

where $B_{\perp 1}$ and S_1 are the component of the magnetic field perpendicular to the target surface and the cross-sectional area of the outer magnets, respectively, $B_{\perp 2}$ and S_2 are the component of magnetic field perpendicular to the target surface and the cross-sectional area of the central magnets. In case of equality of magnetic fluxes of outer and central poles (K=1) all lines of the magnetic field are closed between the poles. For K<1; the magnetic flux at the central pole exceeds the magnetic flux at the outer pole and some of the magnetic lines flow via the central side of the magnetic system [37,38].

The unbalance level of a magnetron can be estimated using a coefficient of geometrical unbalance K_G; according to [39]

$$K_G = \frac{Z}{2R} \quad (2)$$

where R is an average radius of the erosion zone, and the distance Z can be determined by numerical simulation of the magnetic field distribution using the finite-element method.

The introduction of spatial distribution of the magnetic field in closed-field unbalanced magnetron (CFUBM) system is important in determining the optimum condition when employing two magnetrons in plasma sputtering technique as the fundamental goal of using magnetron is to increase the path length of sputtering electrons near the cathode (target). The proposed measuring setup is low-cost, reliable and applicable at working environment of such techniques [39-41].

2. Experimental Part

The magnetron sputtering system used in this work was designed to include vacuum chamber, discharge electrodes and magnetron assembly, vacuum unit, dc power supplies, gas supply system, cooling system and measuring instruments. The system is schematically shown in Fig. (2).

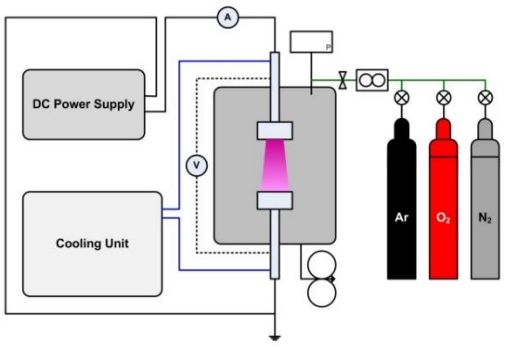

Fig. (2) Schematic diagram of the glow discharge plasma system used in the present work

The vacuum chamber was constructed from stainless steel. It is a cylinder with internal diameter of 35cm, outer diameter of 45cm, and height of 37.5cm. There were four side holes of 10.8cm in diameter on the circumference of the cylinder; one of them was closed with a quartz window, while the other three were closed with glass windows. These windows were mounted by stainless steel flanges each of 21cm in diameter and four screws. They were used for monitoring the discharge and events inside the chamber. Each window was far from the discharge region by a neck of 7.5cm diameter to avoid the effects of heat developed by the glow discharge.

The vacuum chamber was sealed from lower end with a stainless steel flange of 40cm in diameter containing a feedthrough for electrical connections required for experiment. The upper end was sealed with a similar flange but containing two feedthroughs; one for gas inlet and Pirani gauge and the other for the Penning gauge. Both flanges include a central hole for the electrode hollow holder. Rubber O-rings and silicon vacuum grease were used in all sealing points.

Both discharge electrodes were constructed from stainless steel (St. St. 304) hollow disks of 80mm in diameter and 8.5mm in thickness. The electrode was joined to holder of 295mm in length and outer and inner diameters of 16.2mm and 11.6mm, respectively, to include a stainless steel channel of 78.5mm in length and 5.6mm in diameter through which the cooling water was flowed to the inside volume of the electrode. The holder tube includes a 1mm-step screw thread of 25.88mm in length to connect the cooling channel tightly. Figure (3) shows the assembly of the closed-field unbalanced magnetron electrodes.

Two permanent ring magnets were placed at the back side of each electrode to form the magnetron, as shown in Fig.(3), with a separating distance of 1cm. The inner magnet was 12.5mm in height and

31.5mm in diameter with a central hole of 17.5mm in diameter, while the outer magnet was 15.2mm in height and 80mm in diameter with a central hole of 40mm in diameter. Therefore, the two magnets were separated by a distance of 10mm around their opposing surfaces. A metallic disk of 69.7mm in diameter and 2.5mm in thickness was used to choke the outer magnet to prevent the magnetic field lines from extending to the backside of the electrode.

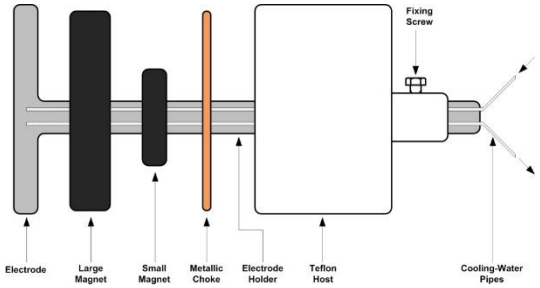

Fig. (3) The assembly of magnetron on each discharge electrode

The design of dual magnetrons proposed in this work provides two concentric regions of high magnetic field intensity on electrode surface. At these regions, the charged particles are totally confined because the particles escaping from the inner region towards the walls of vacuum chamber will lose some energy and then be trapped by the outer region. In conventional configurations, a fraction of charged particles can escape from the confinement region and hence decrease the ionization rate near the cathode.

The advantage of magnetron on the anode is observed in the film deposition of ferromagnetic materials because the magnetic field intensity forces the deposited particles to distribute on the substrate according to its distribution. This makes possible to produce films with selective optical densities to serve multipurpose devices as in the optical data storage applications [42].

In order to prevent any variation in the arrangement of internal components, a teflon host of 100mm diameter and 44.5mm height with a central groove of 84.75mm diameter and 26.3mm depth was used to maintain the magnetron from the backside of the electrode. This piece was locked from movement by cylindrical teflon piece of 37.5mm in diameter and 35.25mm in height containing an M5 screw driven towards the holder tube.

A single-stage rotary pump (Leybold-Heraeus) of 9 m^3/hr pumping speed was used to get pressure down to about 10^{-3} mbar inside the vacuum chamber. A water-cooled diffusion pump was available for use in this work for lower vacuum pressure and connected to the vacuum chamber via a trap. However, all results presented were obtained using the rotary pump only as vacuum pressure of 10^{-2} mbar was easily reached. The minima of Paschen's curves for the inter-electrode distances 2-6 cm were achieved at pressures higher than 10^{-3} mbar. Pirani gauge (down to 10^{-3} mbar) was used.

The electrical power required for generating discharge inside vacuum chamber was provided by a 5 kV dc power supply (Edwards 2A) through high-tension cables. A current-limiting resistance (3.25 kΩ, 1 kW) was connected between the negative terminal of the dc power supply and the cathode inside the vacuum chamber, while the positive terminal of the dc power supply was connected directly to the anode. The output voltage of the power supply could be varied precisely over 0-5 kV to control the current flowing between discharge electrodes. However, the maximum supply voltage did not exceed 800V. Another dc power supply (0-250 V PHYWE-7532) was used to provide bias potential for Langmuir probe measurements. In addition, a third dc power supply (DHF-1502DD, 1.5-15V, 0.6-2A) was used for electrical measurements performed on the samples prepared as photodetectors.

Gas supply unit consists of argon and nitrogen cylinders, flowmeters, gas flow regulators, needle valves and connections and joints. Argon gas of 96% purity and nitrogen gas of 90% purity were used.

A compact unit was used to cool and circulate the room-temperature water through a channel in discharge electrodes. This unit can cool more than 51 liters of distilled water down to about 4°C and circulate it with maximum flow rate of 30 L/min. The temperature inside the chamber was measured by a thermometer located near the wall of the chamber while the temperatures of both electrodes were measured by thermocouples connected to digital instruments. The maximum surface temperature of the substrate placed on the anode was 40-45°C with uncooled circulating water and reasonably reduced with cooled circulating water.

The operating conditions of the system were classified into two groups; constant and variable. The constant operating conditions include inter-electrode distance, vacuum pressure, current limiting resistance, discharge voltage, discharge current, cooling temperature, cooling water flow rate and deposition time. The variable operating conditions include gas pressure and gas flow rate. Varying discharge voltage was almost possible during the operation. In addition, turning the cooling system off would raise the temperature of either electrode to 40-45°C with circulating water, while stopping the circulation of water would raise electrode temperature more (up to 150°C).

3. Results and Discussion

Two teslameters (NV621 and ECOS models) were used to determine the spatial distribution of magnetic field for each magnetron as well as for

both magnetrons simulated to their configuration inside the vacuum chamber. These measurements were performed with with Altay ECOS teslameter.

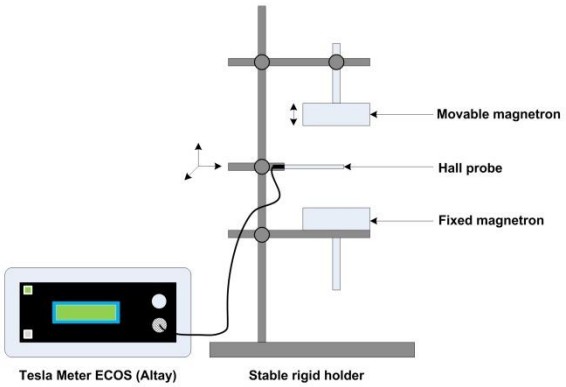

Fig. (4) The experimental setup used for magnetic field distribution measurements

An experimental setup, schematically shown in figure (4) for measuring the magnetic field distribution, was arranged. This experimental setup can simulate the magnetic field distribution between two magnetrons as it makes possible to measure in three dimensions. Results of magnetic field distribution were employed in a modeling process to simulate the spatial profile of the closed-field unbalanced dual magnetrons configuration, which represents a point of novelty over similar works in Iraq.

In this section, the spatial distribution of the magnetic field between two magnetrons in a closed-field unbalanced configuration (CFUBM) was determined. CFUBM's are widely used to generate the discharge plasma employed in sputtering deposition technique to produce low-cost highly-uniform thin films and nanostructures. The spatial distribution is necessary to be introduced in order to optimize the design and operational conditions of such techniques. The experimental setup of this work was reasonably simple, reliable and applicable at working environment. Our results show that the maximum value of the magnetic field due to the interference between the fields of two magnetrons separated by 4 cm was 256 G at the midpoint between them. The design of the magnetron presented in this work showed high uniformity in the configuration of the proposed CFUBM.

The magnetic field of one magnetron was measured as a function of the position of the Hall probe along the circumference of the circular surface of electrode, as shown in figure (5). The magnetic field is at its maximum at the circumference and decreasing when moving inside and nulling at the gap between the outer and inner magnets. Again, the magnetic field grows to reach secondary peak and drops to zero at the central hole of the inner magnet. This uniform behavior is important to ensure the required configuration of the magnetron. If the inner magnet is replaced by a solid one, then the central minimum will disappear and the magnetic field may have a peak comparable to that at the circumference.

In order to determine the optimum distance between two magnetrons, the magnetic field intensity was measured at the midpoint along the distance between the two magnetrons and at 2.2 cm from the edge of the electrode and the results are shown in Figure (6). The maximum was observed at 4 cm, which can be considered as the optimum distance, while the minimum was measured at $\geq$ 8 cm. The diameter of the measuring probe is 0.8 cm, therefore, the minimum distance was 2 cm in order to locate the measuring probe at the midpoint. The behavior shown in figure (6) is attributed to the interference between the lines of the magnetic field, i.e., the maximum interference at the midpoint of 4 cm separation, whereas this interference decreases as the two magnetrons move away from each other reaching to "no interference" condition at $\geq$ 8 cm separation.

The electrons are unable to travel perpendicular to the magnetic field lines over distances greater than Larmor radius, therefore, they are confined. The electric field on the other hand causes the electrons to move in the direction perpendicular to both the electric field and the magnetic field ($\vec{E} \times \vec{B}$ or Hall drift).

The combination of the electron confinement and the $\vec{E} \times \vec{B}$ drift ensures that the electrons have a much longer mean free path in the plasma than in conventional glow discharges, giving rise to more ionization collisions, and consequently higher ion fluxes. These ion fluxes are highest in between the magnets where the regions of maximum sputtering are located. This gives a characteristic feature of conventional planar magnetrons called the racetrack. This racetrack generally limits the complete target utilization, resulting in higher working costs. This problem can be overcome by using rotatable magnetrons. Instead of a cylindrical inner magnet and an outer magnet ring, these magnetrons consist of a central bar shaped magnet surrounded by a rectangular shaped magnet configuration around which a cylindrical target rotates. This greatly enhances the utilization of the target and is therefore much more interesting for industrial applications.

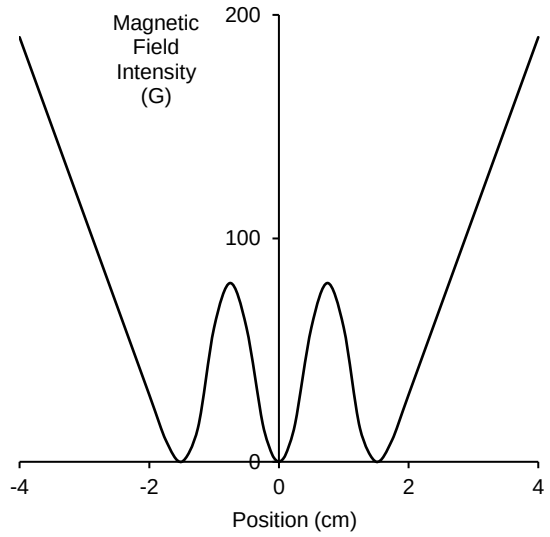

Fig. (5) The magnetic field as a function of the position along the circumference of the circular surface of one magnetron

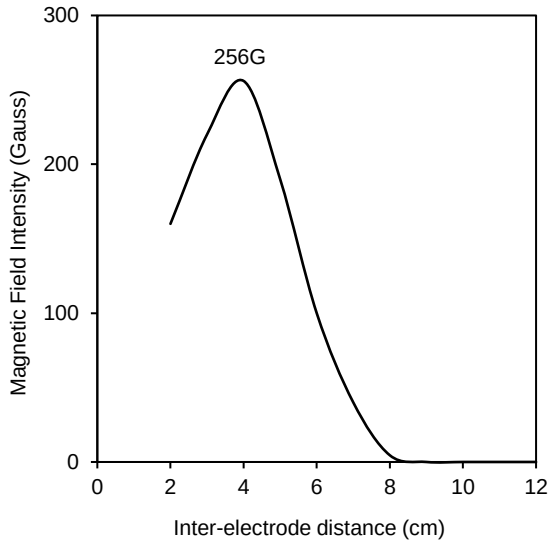

Fig. (6) Variation of magnetic field intensity along the vertical distance separating the two magnetrons

The electrons are assumed to be trapped near the cathode by the magnetic field of the magnetron in order to increase the path length of these electrons. Therefore, the maximum interference between the two fields is not preferred for such purpose because the electrons would not be seized near the cathode. Instead, these electrons may be drifted by the interfered lines away from the cathode.

Figure (7) shows the variation of magnetic field intensity at 4 cm away from the electrode surface along four axes, assigned by 0°, 90°, 180° and 270°, respectively, i.e., each axis is rotated by 90° with respect to the adjacent ones. The profiles shown in the included figures are identical with small differences in the magnetic field intensities. However, the overall profile shows primary maxima at 2.2 and 5.8 cm from starting point at the outer edge of the electrode, while the secondary maxima are shown at 0.6 and 7.4 cm distances. The central part of the profile (1.7cm diameter) show the minimum intensities due to the ring shape of the magnetron. This figure shows uniformity in magnetic field distribution over the magnetron surface.

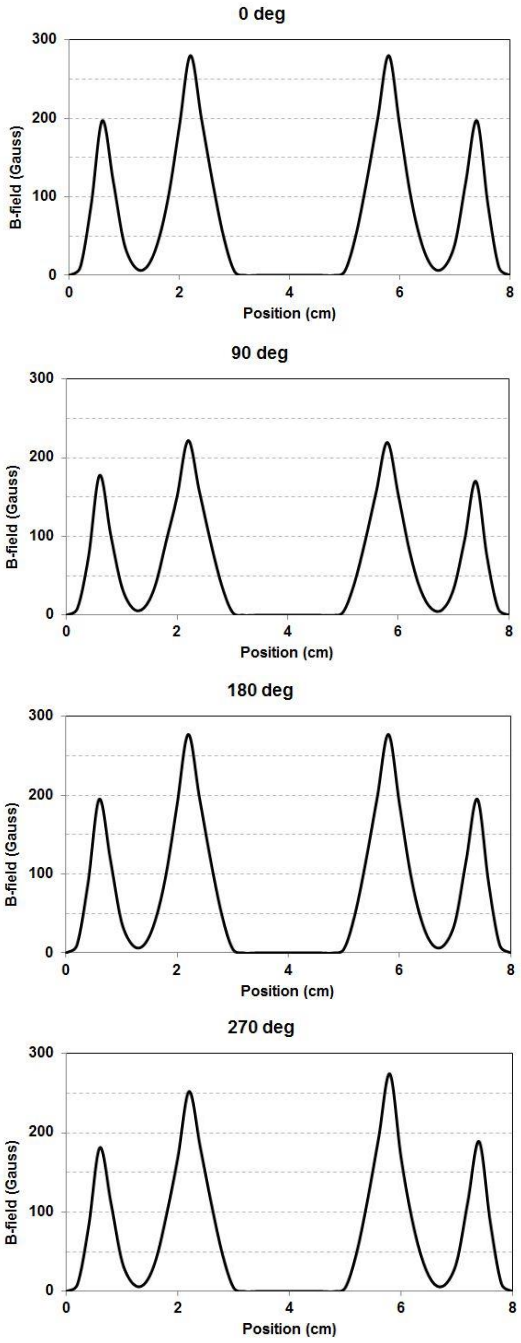

Fig. (7) Variation of magnetic field intensity at 4 cm away from the electrode surface along four axes and the considered strategy of measurement

Sputtering electrons lose their energy to a greater

extent due to ionizing collisions during their drift due to E×B effect. This leads to the decrease in the electron temperature value with the increase in the applied magnetic field strength. The electron temperature is higher near the cathode that is within the magnetic trap, and it goes on decreasing radially away from the cathode as the electrons lose their energy in collision and ionization while travelling radially outward. Near the cathode surface, the electron temperature is high and it decreases away from it. The high value of electron temperature within the E×B trap is due to the confinement of the energetic electrons by the magnetic field. Electron temperature decreases towards the bulk plasma region when one moves away from the cathode surface.

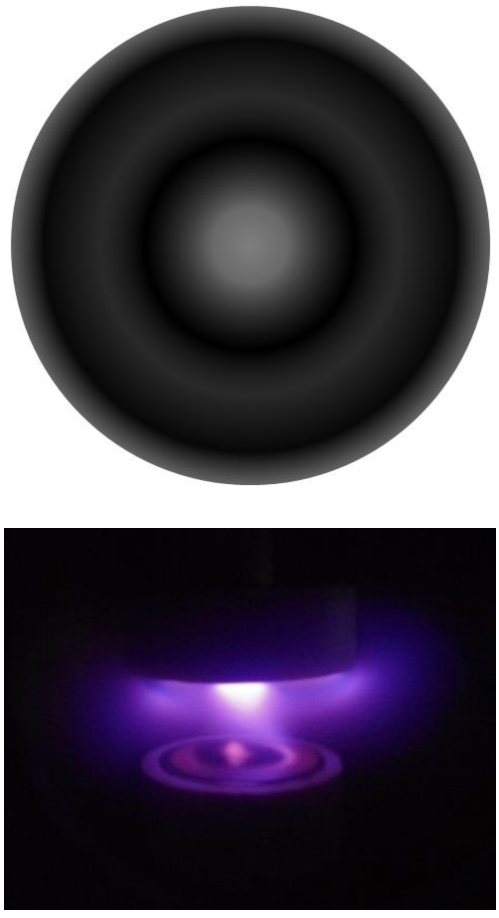

Fig. (8) Spatial distribution of the magnetic field intensity over the magnetron surface at 4cm

It is importance to understand the fundamental phenomena in magnetron discharge. There are a number of models of the magnetron discharge [43-46]. However, most of these models are too complicated to explain the physical meaning, since they deal with the rather special structure of discharge in commercial magnetron devices.

The measurements on magnetic field intensity over the volume between the two magnetrons were modelled and simulated to produce a 3D profile of the magnetic field distribution using Grapher 9.0 and MATLAB 2010 software.

Figure (8) shows the spatial distribution of the magnetic field over the magnetron shown and the gradient in magnetic field is represented by the intensity. Therefore, one can read that, along the radius from the edge to the center of electrode, the intensity is gradually increased to reach its first maximum at about 1cm from the edge, and then gradually decreased to reach its second maximum at about 3cm from the center. The second maximum is higher than the first one as the field lines of the inner magnet is closer to each other when compared to those of the outer one, however, the sputtering electrons are captured by both regions and forced to move with longer paths near the electrode. Values of the magnetic field intensity in this figure represent average of four measurements considered in figure (7).

References

[1] D. Huy Trinh, Nanocrystalline Alumina-Zirconia Thin Films Grown by Magnetron Sputtering, Linköping University, Sweden, p. 1 (2008).

[2] D.R. Gibson, Deposition of multilayer optical coatings using closed field magnetron sputtering, online article (2006).

[3] C. O'Leary, Design, Construction and Characterisation of a Variable Balance Magnetron Sputtering System, Department of Electronic Engineering, Dublin City University, Ireland, p. 15 (1999).

[4] A. Aijaz, Design and Characterization of a Synchronous Co-axial Double Magnetron Sputtering System, MSc thesis, Department of Physics, Chemistry & Biology, Linköping University, Sweden, p. 10, 38 (2009).

[5] P. Vǎsina, Plasma diagnostics focused on new magnetron sputtering devices for thin film deposition, PhD thesis, Universit´e Paris-Sud XI, France & Masaryk University in Brno, Czech Republic, pp. 12-19 (2005).

[6] D. Guttler, An Investigation of Target Poisoning during Reactive Magnetron Sputtering, PhD thesis, Technischen Universitat Dresden, p. 3 (2008).

[7] M. Julfikar Haider, Deposition of Hard and Solid Lubricant (TiN+MoS_x) Coating by Closed-Field Magnetron Sputtering, PhD thesis, School of Mechanical and Manufacturing Engineering,, Dublin University, Ireland, pp. 56-58, 176 (2005).

[8] S. Grigoletto, Synthesis and characterization of titanium carbon nitride films by High Power Impulse Magnetron Sputtering, PhD thesis,

Università Degli Stu Di Di Padova, Italy, p. 7 (2014)
[9] I. Svadkovski, D. Golosov and S. Zavatskiy, Characterisation parameters for unbalanced magnetron sputtering systems, Vacuum, 68, 283–290 (2003).
[10] A.A. Solov'ev, Investigation of Plasma Characteristics in an Unbalanced Magnetron Sputtering System, Plasma Phys. Rep., 35(5), 399–408 (2009).
[11] R.Á. Vargas-Ortiz and F.J. Espinoza-Beltrán, Structural and Chemical Composition of Si-Al Oxy-Nitride Coatings Produced by Reactive DC Magnetron Sputtering, The AZo J. of Materials Online, DOI: 10.2240/azojomo0155.
[12] J.C. da Conceição Lorenzzi, Boron nitride thin films deposited by magnetron sputtering on Si_3N_4, PhD thesis, Universidade de Aveiro, Departamento de Engenharia Cerâmica e do Vidro, pp. 10-16 (2007).
[13] T.E. Sheridan, M.J. Goeckner and J. Goree, Model of energetic electron transport in magnetron discharges, J. Vac. Sci. Technol. A, 8(1), 30-37 (1990).
[14] J. Goree and T. E. Sheridan, Magnetic field dependence of sputtering magnetron efficiency, Appl. Phys. Lett., 59(9), 1052-1054 (1991).
[15] M.B. Hendricks, Effects of ion-induced electron emission on magnetron plasma instabilities, J. Vac. Sci. Technol. A 12, 1408 (1994)
[16] T.E. Sheridan, M.J. Goeckner and J. Goree, Electron velocity distribution functions in a sputtering magnetron discharge for the ExB direction, J. Vac. Sci. Technol. A 16(4), 2173-2176 (1998).
[17] R. Arnell and P. Kelly, Recent advances in magnetron sputtering, Surf. Coat. Technol., 112, 170-176 (1999).
[18] P.J. Kelly and R.D. Arnell, Magnetron sputtering: a review of recent developments and applications, Vacuum, 56, 159-172 (2000).
[19] I. Safi, Recent aspects concerning DC reactive magnetron sputtering of thin films: A review, Surf. Coat. Technol., 127, 203-219 (2000).
[20] C. Engström, Design, plasma studies, and ion assisted thin film growth in an unbalanced dual target magnetron sputtering system with a solenoid coil, Vacuum, 56, 107-113 (2000).
[21] E. Martines, Electrostatic fluctuations in a direct current magnetron sputtering plasma, Phys. of Plasmas, 8(6), 3042-3050 (2001).
[22] C.H. Shon and J.K. Lee, Modeling of Magnetron Sputtering Plasmas, Appl. Surf. Sci., 192, 258-269 (2002).
[23] Gang Xu, Optical investigation of silicon nitride thin films deposited by r.f. magnetron sputtering, Thin Solid Films, 425, 196–202 (2003).
[24] S.A. Awan and R.D. Gould, Conductivity and dielectric properties of silicon nitride thin films prepared by RF magnetron sputtering using nitrogen gas, Thin Solid Films, 423, 267–272 (2003).
[25] I. Levchenko, Stable plasma configurations in a cylindrical magnetron discharge, Appl. Phys. Lett., 85(12), 2202-2204 (2004).
[26] U.H. Kwon, Multi-scale simulation of plasma generation and film deposition in a circular type DC magnetron sputtering system, Thin Solid Films, 475, 17– 23 (2005).
[27] Zh.Q. Yao, Composition, structure and properties of SiNx films fabricated by pulsed reactive closed-field unbalanced magnetron sputtering, Nuclear Instrum. and Methods in Phys. Res., B240, 741–751 (2005).
[28] Junqing Lu, Magnetron target designs to improve wafer edge trench filling in ionized metal physical vapor deposition, Thin Solid Films, 515, 2452–2457 (2006).
[29] K. Mokeddem, M. Aoucher and T. Smail, Hydrogenated amorphous SiN deposited by DC magnetron sputtering, Superlattices and Microstructures, 40, 598–602 (2006).
[30] Zh.Q. Yao, Studies of the composition, tribology and wetting behavior of silicon nitride films formed by pulsed reactive closed-field unbalanced magnetron sputtering, Nuclear Instrum. and Methods in Phys. Res., B242, 33–36 (2006).
[31] Yu Xiang, Investigation of Ti/TiN multilayered films in a reactive mid-frequency dual-magnetron sputtering, Appl. Surf. Sci., 253, 3705–3711 (2007).
[32] A. Batan, Characterisation of the silicon nitride thin films deposited by plasma magnetron, Surf. Interface Anal., 40, 754–757 (2008).
[33] M. Awais, Deposition and characterization of NiO_x coatings by magnetron sputtering, Surf. Coat. Technol., 204(16-17), 2729-2739 (2010).
[34] Asim Aijaz, Dual-magnetron open field sputtering system for sideways deposition of thin films, Surf. Coat. Technol., 204(14), 2165-2169 (2009).
[35] Qusay A. Abbas, R.R. Abdula, B.T. Chiad, The axial profile of plasma characteristics of cylindrical magnetron sputtering device, Iraqi J. of Phys., 8(11), 41-47 (2010).
[36] Baha T. Chied, Rahman R. Abdula, Qusay A. Abbas, Investigation of plasma characteristics of center region of post cylindrical magnetron sputtering device, Iraqi J. of Physics, 8(11), 33-40 (2010).
[37] K. Sarakinos, J. Alami and S. Konstantinidis, High power pulsed magnetron sputtering: A review on scientific and engineering state of the art, Surf. Coat. Technol., 204, 1661–1684 (2010).

[38] A.A. Turkin, On the evolution of film roughness during magnetron sputtering deposition, J. Appl. Phys., 108, 094330 (2010)
[39] R. Raju, Development and characterization of a secondary RF plasma-assisted closed-field dual magnetron sputtering system for optical coatings on large-area substrates, Plasma Sources Sci. Technol., 19, 025011 (2010).
[40] M. Yusupov, Behavior of electrons in a dual-magnetron sputter deposition system: a Monte Carlo model, New J. of Physics, 13, 033018 (2011).
[41] M. Yusupov, Elucidating the asymmetric behavior of the discharge in a dual magnetron sputter deposition system, Appl. Phys. Lett., 98, 131502 (2011).
[42] M. Guziewicz, Electrical and optical properties of NiO films deposited by magnetron sputtering, Optica Applicata, XLI(2), 431-440 (2011).
[43] Sankar M. Borah, Direct Current Magnetron Glow Discharge Plasma Characteristics Study for Controlled Deposition of Titanium Nitride Thin Film, J. of Materials, vol. 2013, article ID 852859.
[44] V. Bouchat, N. Moreau, J.-F. Colomer and S. Lucas, On Some Applications of Nanoparticles Synthesized in the Gas Phase by Magnetron Discharges, J. of Surf. Eng. Mater. and Adv. Technol., 3, 184-189 (2013).
[45] F. Jimenez, S.D. Ekpe and S.K. Dew, Modeling of Low Pressure Magnetron Plasma Discharge, Proc. of the COMSOL Conference 2007, Boston.
[46] Sang-Hun Seo and Hong-Young Chang, Anomalous behaviors of plasma parameters in unbalanced direct-current magnetron discharge, Phys. Plasmas 11, 3595 (2004).

